Optics Letters

Electro-optic dual-comb spectrometer in the thulium amplification band for gas sensing applications

Alexandre Parriaux,* Kamal Hammani, and Guy Millot

Laboratoire Interdisciplinaire Carnot de Bourgogne (ICB), UMR 6303 CNRS—Université Bourgogne Franche-Comté, Dijon, France
**Corresponding author: alexandre.parriaux@u-bourgogne.fr*

Received 9 July 2019; revised 7 August 2019; accepted 8 August 2019; posted 9 August 2019 (Doc. ID 372157); published 26 August 2019

We demonstrate a dual-comb spectrometer based on the direct electro-optic modulation of a continuous-wave laser operating in the thulium amplification band. We show that the emergent two-micrometer technology is already suitable for developing all-fibered dual-comb setups employed here for gas sensing applications. By performing spectroscopic measurements around two micrometers on carbon dioxide, we obtain very good agreement between the experimental results and calculations provided by the HITRAN database. These results pave the way to the extension of electro-optic dual-comb spectrometry in the mid-infrared region.

https://doi.org/10.1364/OL.44.004335

Gas sensing in the mid-infrared (MIR) has recently attracted highly motivated studies, since molecules possess strong rotational–vibrational absorptions in this spectral region. Sensing applications can be performed with several techniques, but setups based on frequency combs present numerous advantages such as high-resolution measurements and real-time recording possibilities in diverse areas of physics [1,2]. Moreover, their use for dual-comb spectroscopy (DCS), i.e., the study of the beating between two mutually coherent combs with slightly different repetition rates [3], still remains topical [4]. In the MIR, frequency combs can be generated with different approaches [5–7], and several setups have recently been proposed for DCS [8–10]. However, this powerful technique generally needs state-of-the-art stabilizations between the combs [11–13], which prevents most outside-the-laboratory applications, although some of them were demonstrated [14].

To overcome this problem, dual-comb systems based on the electro-optic modulation of a continuous-wave (CW) laser can be used, since mutual coherence between the combs is intrinsic to the technique and thus requires no active stabilization [15–17]. However, these setups are generally restrained for applications in the near IR (NIR), generally around 1550 nm where electro-optic modulators have been well optimized for telecommunication applications but where the molecular absorption strengths are weak in that spectral region. Several works managed to overcome this issue by converting the combs in the MIR by means of nonlinear effects such as difference frequency generation in periodic poled lithium niobate crystals [18,19], or fourth-order modulation instability in a highly nonlinear fiber (HNLF) [20], but these techniques, although effective, add a certain complexity to the setup. Moreover, adding a conversion part generally requires a powerful CW laser to induce conversion [18,19], which dramatically increases the cost and the occupied volume of the setup.

In this Letter, we present, to the best of our knowledge, the first all-fibered electro-optic dual-comb spectrometer based on the direct modulation of a CW laser operating in the thulium amplification band, which is one of the last steps towards the MIR region. We show that the emerging two-micrometer technology can be used for designing setups almost equivalent to what is already made around 1550 nm despite their less efficient characteristics. To illustrate the efficiency of the setup, we perform DCS around two micrometers, and comparisons with calculations provided by the HITRAN database of molecular absorption lines show very good agreement.

The all-fibered dual-comb setup for gas sensing in the thulium amplification band is presented in Fig. 1. Although the architecture follows the one presented in Ref. [16], which was also used in Refs. [18,20], here the components are specifically designed for the two-micrometer spectral region. More precisely, we start with a tunable CW laser operating between 1890 nm and 2020 nm that is amplified at a power of 150 mW with a thulium-doped fiber amplifier (TDFA). These amplifiers provide a large amplification bandwidth from 1850 nm to around 2050 nm and thus define the working range of the setup. The CW laser, fixed around 2000 nm for later spectroscopic applications, is divided into two arms with a 50/50 coupler that feeds in each arm an intensity modulator (IM, iXblue MX2000-LN-10) for generating two mutually coherent combs. The IMs are driven by an electrical pulse generator delivering 50 ps full width at half-maximum (FWHM) Gaussian pulses. The repetition rate f_{rep} is provided by a sinusoidal generator and is easily tunable between 100 MHz and 1 GHz. In the following, we set the repetition rate of the combs to $f_{rep} = 300$ MHz and $f_{rep} + \Delta f_{rep} = 300.057$ kHz. An example of temporal

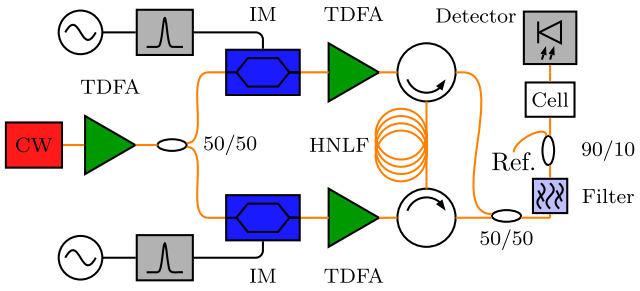

Fig. 1. Schema of the all-fibered dual-comb setup based on the direct modulation of a continuous-wave laser operating in the thulium amplification band for spectroscopic applications. CW, continuous wave; TDFA, thulium-doped fiber amplifier; IM, intensity modulator; HNLF, highly nonlinear fiber.

output recorded with a real-time oscilloscope after one IM is presented in Fig. 2 and shows a Gaussian pulse of 63 ps FWHM with a standard deviation of 0.93% compared to a pure Gaussian form fitted to the experimental data. The temporal profile has a width slightly larger than the FWHM of the electrical pulse, since the bandwidth of the IMs used is smaller than 20 GHz. Hence, our IMs do not transcribe exactly the electrical pulses, and the optical output is found to be slightly broadened. Note that two-micrometer IMs with a bandwidth larger than 40 GHz are commercially available and could thus generate shorter pulses.

Considering the long pulses obtained, the associated spectrum is too narrow for spectroscopic applications and thus needs to be broadened. Therefore, at the output of the IMs, both combs are amplified with two distinct TDFAs up to a peak power $P = 12$ W, and using two circulators, the combs are then counter-progatively launched in a 500 m HNLF delivered by Sumitomo Electrics. We estimated the parameters of the fiber at 1980 nm to be $D = -0.8$ ps $\cdot$ nm^{-1} $\cdot$ km^{-1} for the dispersion coefficient, $\gamma = 21$ W^{-1} $\cdot$ km^{-1} for the Kerr coefficient, and $\alpha = 15$ dB $\cdot$ km^{-1} for the linear loss coefficient. This particular HNLF was chosen due to the presence of a normal dispersion regime around two micrometers, which avoids detrimental effects such as second-order modulation instability that could deteriorate the intrinsic mutual coherence between the combs. The broadening is then made in a pure nonlinear

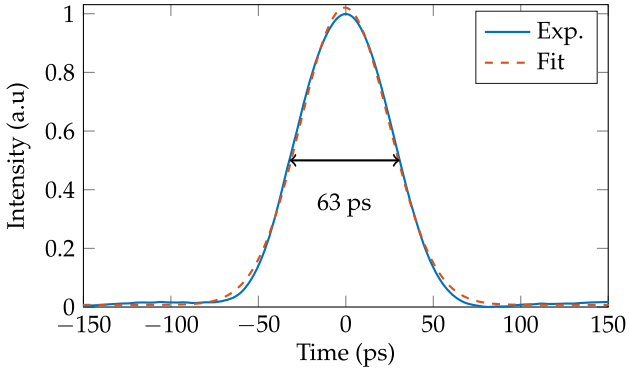

Fig. 2. Temporal trace of pulses obtained after the intensity modulation of a continuous-wave laser compared with the least-squared fit of a Gaussian profile.

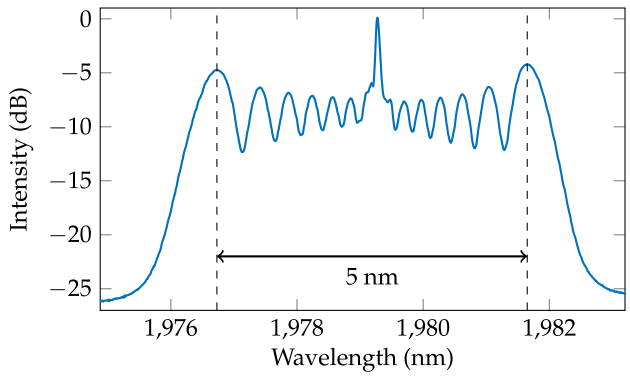

Fig. 3. Recorded spectrum at the output of a 500 m long highly nonlinear fiber of parameters $D = -0.8$ ps $\cdot$ nm^{-1} $\cdot$ km^{-1}, $\gamma = 21$ W^{-1} $\cdot$ km^{-1}, and $\alpha = 15$ dB $\cdot$ km^{-1} at 1980 nm. The spectral broadening of 63 ps Gaussian pulses is obtained for a peak power $P = 12$ W and shows a 5 nm wide spectrum.

self-phase modulation (SPM) regime, and the spectrum presents strong oscillations [21]. This can be observed with an optical spectrum analyzer, as presented in Fig. 3. The recorded spectrum shows a span of more than 5 nm, which is in good agreement with the theoretical expression of the maximal spectral width obtainable in a pure SPM regime [21]. Contrary to usually performed spectral broadening at 1550 nm, here the dispersion coefficient of the HNLF is too low in absolute values and the losses too high for broadening the spectrum by dispersive shock waves, which would have flattened the spectrum [16–18,22]. However, this fact should be put into perspective, since the low extinction ratio of the IMs estimated around 20 dB would also create strong oscillations in the spectrum if the phenomenon of dispersive shock waves could occur [22].

After spectral broadening, both combs are coupled with a 50/50 coupler and filtered to suppress one side of the spectrum in relation to the CW central wavelength. This is done to avoid the overlapping in the radio-frequency (RF) domain of the optical comb line beatings coming from both sides of the spectrum, which creates ambiguities. Note that an acousto-optic modulator could have been used to solve this aliasing problem [16–18]. The filtering is also performed to remove the amplified spontaneous emission coming from the TDFAs and to increase the signal-to-noise ratio [23].

Once filtered, the coupled combs are sent on a two-micrometer InGaAs photodiode (EOT ET-5000F), whose signal is digitized using an oscilloscope. This reveals an interferogram for which Fourier transformation gives a down-converted comb in the RF domain. An example of a RF comb obtained by Fourier transforming 2.1 ms long interferograms with 2^{17} points averaged over 420 ms with a sampling time of 8 ns and a dynamic of 8 bit is shown in Fig. 4(a). We observe that the spectrum is composed of more than 700 resolved lines with a measured dynamic exceeding 20 dB over most of the width of the comb. We can observe that the envelope of the RF comb is smoother than the spectrum presented in Fig. 3, which is due to small asymmetries between the two arms of the spectrometer. Indeed, each IM does not have the exact same extinction ratio, the TDFAs are not exactly equivalent, etc., which leads to small differences in the optical spectrum,

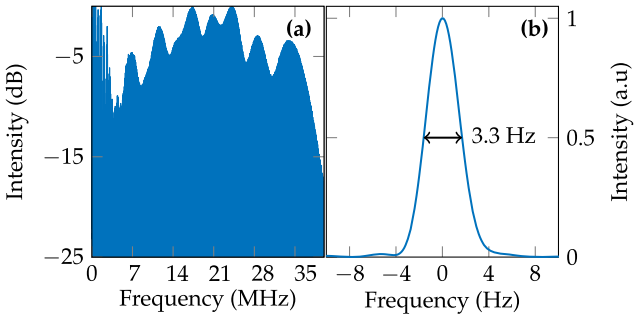

Fig. 4. (a) Example of a down-converted comb in the radio-frequency domain. (b) Zoom on a particular line of the comb obtained by Fourier transformation of a 500 ms long interferogram revealing a full width at half-maximum of 3.3 Hz.

particularly in the characteristics of the sidelobes generated by SPM. Thus, when the combs are combined, the obtained RF spectrum does not exactly reflect the optical spectra. However, the asymmetries are not especially detrimental, since they can be exploited to minimize the strong oscillations due to the SPM effect. This can be done empirically by slightly adjusting the polarization state of the combs in the setup, the power delivered by the TDFAs, and the position of the filter. All of this makes the envelope of the RF comb smoother but also avoids RF zones with poor dynamics that would be less exploitable.

Using a 500 ms long recorded interferogram that is Fourier transformed, we can zoom on a particular line of the comb, which is presented in Fig. 4(b). The RF line possesses a 3.3 Hz FWHM, which is equal to 18 kHz in the optical domain, showing an excellent mutual coherence between the combs. Note that this value is a maximum value limited by the recorded time of the interferogram. Compared to the equivalent setup at 1550 nm [16], the conversion of this same setup around 3300 nm by difference frequency generation [18] or around two micrometers by modulation instability [20], the FWHMs of the RF lines are very close (13 kHz, 6.9 kHz, and 18 kHz, respectively).

We now perform DCS to evaluate the potential of the setup for gas sensing applications. As shown in Fig. 1, a 78.1 cm long fibered cell is added at the output of the dual-comb spectrometer between the filter and the photodiode. Before the cell, a 90/10 coupler is placed to collect 10% of the signal that will be used as a reference arm. The signal of the reference arm is also directed towards a photodiode so that the absorption and reference signals are recorded at the same time. This is done to avoid any spectral fluctuations of the comb optical spectra between the measurements of the absorption and reference signals, which could be much more detrimental compared to the case of having a flat-topped optical spectrum [16,18,20].

The cell is filled with gaseous carbon dioxide in natural isotopic abundance at a pressure of 520 mbar. By setting the initial CW laser around 1996.3 nm, we observe several lines of the $^{12}CO_2$ R branch associated with the $\nu_1 + 2\nu_2 + \nu_3$ rotational–vibrational band plus several lines of the $^{13}CO_2$ R branch associated with the $2\nu_1 + \nu_3$ band. An example of recorded absorption spectrum over almost 2 nm is presented in Fig. 5 (a) (top). A computed absorption spectrum using calculations provided by the HITRAN database is shown in Fig. 5(a) (middle) [24], and the difference between the

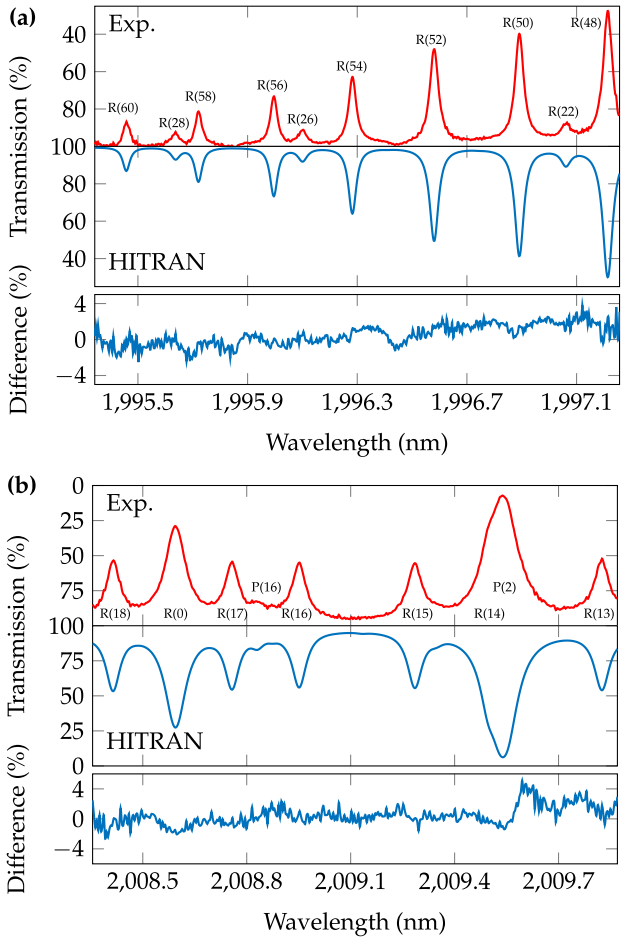

Fig. 5. (a) Experimental absorption spectrum of CO_2 in natural isotopic abundance obtained around 1996.3 nm at a pressure of 520 mbar (top) compared with a computed spectrum using calculations provided by the HITRAN database (middle) and difference between the two sets of data (bottom). (b) Same as (a) but with a spectrum obtained around 2009.1 nm.

experimental and computed data are shown in Fig. 5(a) (bottom). The experimental absorption spectrum is obtained by translating the recorded RF spectrum back in the wavelength domain using the demultiplication factor of the dual-comb setup, which is given by $\frac{f_{rep}}{\Delta f_{rep}}$. Finally, since the dual-comb spectrometer operates in a free-running mode; the wavelength calibration of the experimental data was made by matching the central frequency of the R(54) line with the one provided by the HITRAN database. Note that the calibration could have been made by referencing the initial CW laser to an optical clock. The standard deviation associated with the difference is 1.78%, which shows a very good agreement between both sets of data.

As mentioned earlier, the initial CW laser is tunable between 1890 nm and 2020 nm. Therefore, by slightly tuning the central wavelength of the CW laser up to 2009.1 nm, we can observe the $^{12}CO_2$ P + R branches junction of the $\nu_1 + 2\nu_2 + \nu_3$ band. An example of recorded absorption spectrum is presented in Fig. 5(b) (top), and lines coming from the $^{12}CO_2$ R branch associated with the $\nu_1 + 3\nu_2 + \nu_3$ band

plus a line coming from the $^{13}CO_2$ P branch associated with the $2\nu_1 + \nu_3$ band are observable. As previously, a computed absorption spectrum from the HITRAN database is shown in Fig. 5(b) (middle), and the difference between both sets of data are shown in Fig. 5(b) (bottom). Here, the calibration is made by matching the central wavelength of the R(17) line, and the standard deviation associated with the difference is 1.25%, which also shows a very good agreement between both sets of data. Note that we checked the possibility of observing the $2\nu_1 + \nu_3$ band located around 1960 nm (not shown here) by tuning the CW laser adequately. From all of these results, we obtained a minimum intensity of detection of the setup equal to 5×10^{-24} cm per molecule.

In this Letter, we presented an all-fibered dual-comb spectrometer based on the direct electro-optic modulation of a CW laser operating in the thulium amplification band for gas sensing applications. We showed that the two-micrometer technology is suitable for developing a dual-comb spectrometer based on IMs despite their less efficient features compared to components operating near 1550 nm (bandwidth, extinction ratio, etc.). Knowing the thulium amplification bandwidth is limited to a few tens of nanometers above 2000 nm, the presented setup is also limited in its sensing applications. However, the simple exchange for holmium-doped fiber amplifiers with an adequate CW laser could extend the working range up to 2150 nm [25,26], enabling, for instance, the sensing of the $4\nu_2 + \nu_3$ band of $^{12}CO_2$ and the $\nu_1 + 2\nu_2 + \nu_3$ band of $^{13}CO_2$, but also other gases such as N_2O.

At the expense of the all-fibered feature, setups based on the direct modulation of a CW laser could lead to higher wavelength operations, since optical modulators have been reported working in the MIR up to 8 μm using Si-on-$LiNbO_3$ [27], black phosphorus [28], or Ge-on-Si technology [29]. Spectral broadening in this region could be performed in exotic fibers [30] or in waveguides [31]. We believe that the presented results can open up new opportunities in designing compact and fast analysis spectrometers in wavelength regions very suitable for gas sensing applications.

Funding. Conseil régional de Bourgogne Franche-Comté; iXCore Research Fondation; project ISITE-BFC (ANR-15-IDEX-0003); EIPHI Graduate School (ANR-17-EURE-0002); Institut Universitaire de France (IUF).

REFERENCES

1. T. W. Hänsch, Rev. Mod. Phys. **78**, 1297 (2006).
2. J. L. Hall, Rev. Mod. Phys. **78**, 1279 (2006).
3. S. Schiller, Opt. Lett. **27**, 766 (2002).
4. I. Coddington, N. Newbury, and W. Swann, Optica **3**, 414 (2016).
5. A. Schliesser, N. Picqué, and T. W. Hänsch, Nat. Photonics **6**, 440 (2012).
6. G. Soboń, T. Martynkien, P. Mergo, L. Rutkowski, and A. Foltynowicz, Opt. Lett. **42**, 1748 (2017).
7. R. Rockmore, A. Laurain, J. V. Moloney, and R. J. Jones, Opt. Lett. **44**, 1797 (2019).
8. M. I. Kayes, N. Abdukerim, A. Rekik, and M. Rochette, Opt. Lett. **43**, 5809 (2018).
9. R. Liao, Y. Song, W. Liu, H. Shi, L. Chai, and M. Hu, Opt. Express **26**, 11046 (2018).
10. L. A. Sterczewski, J. Westberg, M. Bagheri, C. Frez, I. Vurgaftman, C. L. Canedy, W. W. Bewley, C. D. Merritt, C. S. Kim, M. Kim, J. R. Meyer, and G. Wysocki, Opt. Lett. **44**, 2113 (2019).
11. G. Ycas, F. R. Giorgetta, E. Baumann, I. Coddington, D. Herman, S. A. Diddams, and N. R. Newbury, Nat. Photonics **12**, 202 (2018).
12. A. V. Muraviev, V. O. Smolski, Z. E. Loparo, and K. L. Vodopyanov, Nat. Photonics **12**, 209 (2018).
13. Z. Chen, T. W. Hänsch, and N. Picqué, Proc. Natl. Acad. Sci. USA **116**, 3454 (2019).
14. G. Ycas, F. R. Giorgetta, K. C. Cossel, E. M. Waxman, E. Baumann, N. R. Newbury, and I. Coddington, Optica **6**, 165 (2019).
15. D. A. Long, A. J. Fleisher, K. O. Douglass, S. E. Maxwell, K. Bielska, J. T. Hodges, and D. F. Plusquellic, Opt. Lett. **39**, 2688 (2014).
16. G. Millot, S. Pitois, M. Yan, T. Hovhannisyan, A. Bendahmane, T. W. Hänsch, and N. Picqué, Nat. Photonics **10**, 27 (2016).
17. V. Durán, P. A. Andrekson, and V. Torres-Company, Opt. Lett. **41**, 4190 (2016).
18. M. Yan, P.-L. Luo, K. Iwakuni, G. Millot, T. W. Hänsch, and N. Picqué, Light Sci. Appl. **6**, e17076 (2017).
19. B. Jerez, P. Martín-Mateos, F. Walla, C. de Dios, and P. Acedo, ACS Photonics **5**, 2348 (2018).
20. A. Parriaux, K. Hammani, and G. Millot, Commun. Phys. **1**, 17 (2018).
21. G. Agrawal, *Nonlinear Fiber Optics*, 5th ed., Optics and Photonics Series (Academic, 2012).
22. A. Parriaux, M. Conforti, A. Bendahmane, J. Fatome, C. Finot, S. Trillo, N. Picqué, and G. Millot, Opt. Lett. **42**, 3044 (2017).
23. I. Coddington, W. C. Swann, and N. R. Newbury, Phys. Rev. Lett. **100**, 013902 (2008).
24. http://www.cfa.harvard.edu/hitran/.
25. N. Simakov, Z. Li, Y. Jung, J. M. O. Daniel, P. Barua, P. C. Shardlow, S. Liang, J. K. Sahu, A. Hemming, W. A. Clarkson, S.-U. Alam, and D. J. Richardson, Opt. Express **24**, 13946 (2016).
26. R. E. Tench, C. Romano, G. M. Williams, J. Delavaux, T. Robin, B. Cadier, and A. Laurent, J. Lightwave Technol. **37**, 1434 (2019).
27. J. Chiles and S. Fathpour, Optica **1**, 350 (2014).
28. R. Peng, K. Khaliji, N. Youngblood, R. Grassi, T. Low, and M. Li, Nano Lett. **17**, 6315 (2017).
29. T. Li, M. Nedeljkovic, N. Hattasan, W. Cao, Z. Qu, C. G. Littlejohns, J. S. Penades, L. Mastronardi, V. Mittal, D. Benedikovic, D. J. Thomson, F. Y. Gardes, H. Wu, Z. Zhou, and G. Z. Mashanovich, Photon. Res. **7**, 828 (2019).
30. A. Lemière, F. Désévédavy, B. Kibler, P. Mathey, G. Gadret, J.-C. Jules, C. Aquilina, P. Béjot, F. Billard, O. Faucher, and F. Smektala, Laser Phys. Lett. **16**, 075402 (2019).
31. N. Nader, D. L. Maser, F. C. Cruz, A. Kowligy, H. Timmers, J. Chiles, C. Fredrick, D. A. Westly, S. W. Nam, R. P. Mirin, J. M. Shainline, and S. Diddams, APL Photonics **3**, 036102 (2018).